

Novel neutron resonance mode in $d_{x^2-y^2}$ superconductors

Ilya Eremin^{1,*}, Dirk K. Morr^{1,2}, Andrey V. Chubukov³, Karl Bennemann¹, and Michael R. Norman⁴

¹ *Institute für Theoretische Physik, Free Universität Berlin, D-14195, Berlin, Germany*

² *Department of Physics, University of Illinois at Chicago, Chicago, IL 60607*

³ *Department of Physics, University of Wisconsin, Madison, WI 53706*

⁴ *Materials Science Division, Argonne National Laboratory, Argonne, IL 60439*

(Dated: February 2, 2008)

We show that a new resonant magnetic excitation at incommensurate momenta, observed recently by inelastic neutron scattering experiments on $\text{YBa}_2\text{Cu}_3\text{O}_{6.85}$ and $\text{YBa}_2\text{Cu}_3\text{O}_{6.6}$, is a *spin exciton*. Its location in the magnetic Brillouin zone and its frequency are determined by the momentum dependence of the particle-hole continuum. We identify several features that distinguish this novel mode from the previous resonance mode observed near $\mathbf{Q} = (\pi, \pi)$, such as its intensity maximum which occurs in a different part of the magnetic Brillouin zone.

PACS numbers: 71.10.Ca, 74.20.Fg, 74.25.Ha, 74.72.Bk

While it seems established that the resonance peak is a universal feature of the high-temperature superconductors [1, 2, 3], its origin, its role for the pairing process, and the effects arising from its interactions with electrons are still intensively debated [4]. The peak's intensity is the highest at $\mathbf{Q} = (\pi, \pi)$ and in $\text{YBa}_2\text{Cu}_3\text{O}_{6+x}$ (YBCO), where it was studied in great detail, its frequency $\Omega_{res}(\mathbf{Q})$ follows the same doping dependence as T_c , with $\Omega_{res}(\mathbf{Q}) \approx 41$ meV near optimal doping. As one moves away from \mathbf{Q} , the peak disperses downwards and its intensity decreases rapidly, vanishing around $\mathbf{Q}_0 = (0.8\pi, 0.8\pi)$. The doping dependence of $\Omega_{res}(\mathbf{Q})$, the downward dispersion of the resonance, and the fact that \mathbf{Q}_0 coincides with the distance between nodal (diagonal) points on the Fermi surface are consistent with the theoretical idea that the resonance peak is a particle-hole bound state below the spin gap (a spin exciton) [5] (for a review of other theoretical scenarios, see Ref. [6]).

Recent inelastic neutron scattering (INS) experiments on $\text{YBa}_2\text{Cu}_3\text{O}_{6.85}$ [7] in the superconducting (SC) state detected a new resonant magnetic excitation at incommensurate momenta, but at frequencies *larger* than $\Omega_{res}(\mathbf{Q})$. A similar result was obtained for underdoped $\text{YBa}_2\text{Cu}_3\text{O}_{6.6}$ [8]. This new resonance mode is particularly pronounced along the diagonal of the magnetic Brillouin zone (MBZ) at $\mathbf{q} \lesssim \mathbf{Q}_0$. It was suggested [7] that this new resonance is a particle-hole bound state with an upward dispersion originating at \mathbf{Q} (see Fig. 5a in Ref. [7]).

In this Letter, we show both analytically and numerically that the new resonance mode is indeed a spin exciton that emerges below T_c due to a feedback effect on the collective spin excitations arising from the opening of the SC gap in a $d_{x^2-y^2}$ superconductor. We demonstrate that the new resonance appears only at momenta less than \mathbf{Q}_0 , and is separated from the previous resonance by a region near \mathbf{Q}_0 in which no resonance exists (the “silent band” of Ref. [7]). Thus, the new resonance does *not* form an upward dispersing branch originating

at \mathbf{Q} . We identify several qualitative features that distinguish this new resonance (the Q^* mode) from the old one (the Q mode). In particular, we show that while the intensity of the Q mode is largest along $\mathbf{q} = (\pi, \eta\pi)$ and $\mathbf{q} = (\eta\pi, \pi)$, the Q^* mode has its largest intensity along the MBZ diagonal.

We begin by presenting our numerical analysis of the new Q^* mode. Its emergence can be understood within an RPA approach for which the spin susceptibility is given by

$$\chi(\mathbf{q}, \omega) = \frac{\chi_0(\mathbf{q}, \omega)}{1 - g(\mathbf{q})\chi_0(\mathbf{q}, \omega)} \quad (1)$$

where $g(\mathbf{q})$ is the fermionic four-point vertex, and $\chi_0(\mathbf{q}, \omega)$ is the free-fermion susceptibility, which in the SC state is given by the sum of two single bubble diagrams consisting of either normal or anomalous Greens functions [5, 9]. For our numerical calculation of $\chi_0(\mathbf{q}, \omega)$, we used a SC gap with $d_{x^2-y^2}$ symmetry and a normal state tight binding dispersion

$$\epsilon_{\mathbf{k}} = -2t(\cos k_x + \cos k_y) - 4t'\cos k_x \cos k_y - \mu \quad (2)$$

with $t = 250$ meV, $t'/t = -0.4$, and $\mu/t = -1.083$. The Fermi surface (FS) obtained from Eq. (2) is shown in Fig. 3(a). It describes well the FS measured by photoemission experiments on $\text{Bi}_2\text{Sr}_2\text{CaCu}_2\text{O}_{8+\delta}$ [10].

Our main results are presented in Figs. 1 and 2, in which we plot $\text{Im}\chi(\mathbf{q}, \omega)$, obtained from a numerical evaluation of Eq.(1), along $\mathbf{q} = \eta(\pi, \pi)$ in the SC state. The intensity plot of $\text{Im}\chi(\mathbf{q}, \omega)$ shown in Fig. 1 possesses all salient features observed in the INS experiments. First, we identify a downward dispersion of the Q mode (indicated by a red arrow). Second, the Q^* mode (indicated by a yellow arrow) is located at frequencies larger than the frequency of the Q mode at (π, π) , and is confined to a small region of momentum space near \mathbf{Q}_0 . The momentum position of the Q^* mode is almost independent of energy. Third, there exists a region in momentum space around \mathbf{Q}_0 that separates the Q mode from the Q^*

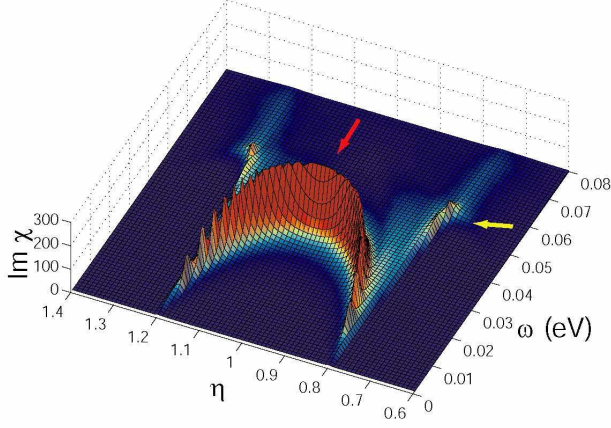


FIG. 1: (color) RPA results for magnetic excitations in a $d_{x^2-y^2}$ superconductor. $\text{Im}\chi$ obtained from Eq. (1) as a function of momentum (along $\mathbf{q} = \eta(\pi, \pi)$) and frequency in the SC state. We used $\Delta_{\mathbf{k}} = \Delta_0(\cos k_x - \cos k_y)/2$ with $\Delta_0 = 42$ meV, and $g(\mathbf{q}) = g_0[1 - 0.1(\cos q_x + \cos q_y)]$, with $g_0 = 0.573$ eV in order to reproduce the correct energy position of the Q^* mode near $0.8(\pi, \pi)$ and the Q mode at (π, π) .

one (the “silent band” of Ref. [7]). Note, that as \mathbf{Q}_0 is approached from (π, π) , the Q mode frequency, $\Omega_{res}(\mathbf{q})$, as well as its intensity, rapidly decreases. In Fig. 2 we present $\text{Im}\chi$ along $\mathbf{q} = \eta(\pi, \pi)$ for several frequencies. We clearly see that the two modes are separated in momentum and frequency space. The shaded area in Fig. 2 represents the silent band, in which $\text{Im}\chi$ is strongly reduced from its resonance values. We also find that the position of the Q^* mode is almost frequency independent, with a maximum intensity at $\omega \approx 54$ meV, in agreement with the experimental observations (see Fig. 2a of Ref. [7]).

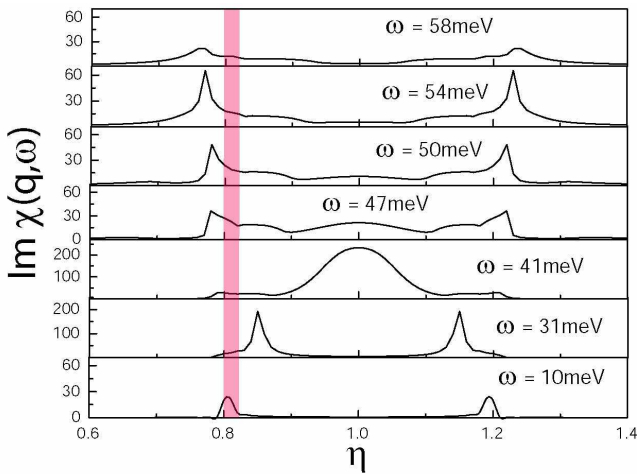


FIG. 2: $\text{Im}\chi(\mathbf{q}, \omega)$ along $\mathbf{q} = \eta(\pi, \pi)$ for several frequencies. The position of the silent band is indicated by the shaded area. These results reproduce the experimental INS data, see Fig. 2(a) in Ref. [7].

In what follows, we discuss the physical origin of our results. We begin by reviewing the emergence of the Q mode. Its origin lies in a feedback effect on the spin excitation spectrum (i.e., on χ_0) due to the opening of the SC gap. This feedback effect is universal in that it only requires that the FS possesses points, \mathbf{k} and \mathbf{k}' , that can be connected by \mathbf{Q} (so-called “hot spots”) and that $\text{sgn}(\Delta_{\mathbf{k}}) = -\text{sgn}(\Delta_{\mathbf{k}'})$. To demonstrate the universality of the resonance mode, we rewrite the denominator of Eq. (1) as

$$\xi_{\mathbf{Q}}^{-2} - g(\mathbf{Q})\Delta\chi_0(\mathbf{Q}, \Omega) \quad (3)$$

where $\xi_{\mathbf{Q}}^{-2} = 1 - g(\mathbf{Q})\chi_0^{ns}(\mathbf{Q}, 0)$ and $\Delta\chi_0(\mathbf{Q}, \Omega) = \chi_0(\mathbf{Q}, \Omega) - \chi_0^{ns}(\mathbf{Q}, 0)$. The main contribution to the static normal state susceptibility $\chi_0^{ns}(\mathbf{Q}, 0)$ comes from high internal frequencies in the fermionic bubble. This implies that χ_0^{ns} and thus $\xi_{\mathbf{Q}}^{-2}$ are non-universal quantities that depend on the details of the band structure. However, the appearance of the resonance mode only requires $\xi_{\mathbf{Q}}^{-2} > 0$, which is satisfied in the paramagnetic state. In contrast, $\Delta\chi_0(\mathbf{Q}, \Omega)$ is *universal* since its main contribution comes from small internal frequencies of order Δ . $\Delta\chi_0$ can therefore be evaluated by simply linearizing the fermionic dispersion near \mathbf{k} and \mathbf{k}' . The integration over momentum [11] yields at $T = 0$

$$\Delta\chi_0(\mathbf{Q}, \Omega) = -i\frac{\gamma_{\mathbf{Q}}^{NS}}{16} \sum_{\{\mathbf{k}, \mathbf{k}'\}} \int_{-\infty}^{\infty} d\omega \times \left(1 - \frac{\omega_+ \omega_- + \Delta_{\mathbf{k}} \Delta_{\mathbf{k}'}}{\sqrt{\omega_+^2 - \Delta_{\mathbf{k}}^2} \sqrt{\omega_-^2 - \Delta_{\mathbf{k}'}^2}} \right) \quad (4)$$

where $\omega_{\pm} = \omega \pm \Omega/2$, and the summation runs over all pairs of FS points \mathbf{k} and \mathbf{k}' separated by \mathbf{Q} . There are eight fermionic scattering processes from \mathbf{k} to \mathbf{k}' in the first zone. The momenta \mathbf{k} involved are those in which the boundary of the magnetic zone (defined by $\cos k_x = -\cos k_y$) crosses the FS. Two of these scattering processes are direct with $\mathbf{k} - \mathbf{k}' = \mathbf{Q}$, two involve umklapp scattering with $\mathbf{k} - \mathbf{k}' = \mathbf{Q} - (2\pi, 2\pi)$, and four involve umklapp scattering with $\mathbf{k} - \mathbf{k}' = \mathbf{Q} - (2\pi, 0)$ and $\mathbf{k} - \mathbf{k}' = \mathbf{Q} - (0, 2\pi)$. A pair of FS points that are connected by direct scattering via \mathbf{Q} is shown in Fig. 3(a) (\mathbf{Q} is represented by a dashed arrow).

In the normal state, all eight processes equally contribute to $\Delta\chi_0(\mathbf{Q}, \Omega)$, and one obtains from Eq. (4) $\Delta\chi_0(\mathbf{Q}, \Omega) = -i\gamma_{\mathbf{Q}}^{NS}\Omega$ which identifies $\gamma_{\mathbf{Q}}^{NS}$ with the Landau damping rate [12]. In the superconducting state, $\Delta\chi_0$ becomes a complex function. According to Eq. (4), its imaginary part vanishes below a critical frequency $\Omega_c(\mathbf{Q}) = |\Delta_{\mathbf{k}}| + |\Delta_{\mathbf{k}'}|$, which is the same for all eight scattering channels. The $d_{x^2-y^2}$ symmetry of the SC gap implies $\Delta_{\mathbf{k}} = -\Delta_{\mathbf{k}'}$, resulting in a discontinuous jump of $\text{Im}\chi_0$ at $\Omega_c(\mathbf{Q})$ from zero to $\pi\gamma_{\mathbf{Q}}^{NS}|\Delta_{\mathbf{k}}|$ [5]. Simultaneously, $\text{Re}\Delta\chi_0(\mathbf{Q}, \Omega) > 0$ is non-zero, diverges logarithmically at $\Omega_c(\mathbf{Q})$, and scales as Ω^2 at small frequencies.

$\text{Re}\Delta\chi_0$ therefore varies between 0 at $\Omega = 0$ and ∞ at $\Omega = \Omega_c$. Since $\xi_Q^{-2} > 0$, one finds that for any positive g_Q , $\chi(Q, \Omega)$ [Eq. (1)] acquires a pole at a frequency $\Omega_{res} < \Omega_c(Q)$ where $\text{Re}\Delta\chi_0(Q, \Omega_{res}) = \xi_Q^{-2}/g_Q$ and $\text{Im}\Delta\chi_0(Q, \Omega_{res}) = 0$. $\text{Im}\chi$ thus exhibits a δ -function at Ω_{res} , representing a spin exciton below the particle-hole (p-h) continuum.

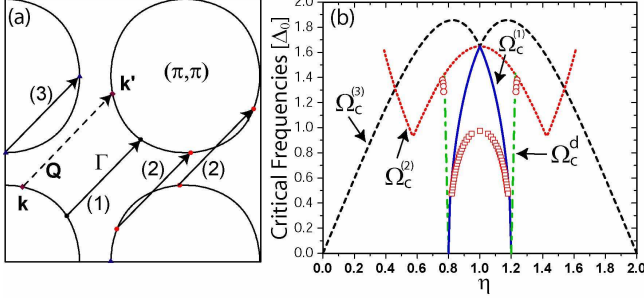


FIG. 3: (a) FS of Eq. (2) and magnetic scattering vectors. (b) Momentum dependence of the critical frequencies $\Omega_c^{(i)}$ ($i = 1, 2, 3$) and the direct gap Ω_c^d along $\mathbf{q} = \eta(\pi, \pi)$ (see text). The open squares (circles) represent the position of the Q (Q^*) resonance.

We next consider the dispersion of the exciton. For $\mathbf{q} \neq \mathbf{Q}$, the degeneracy of the scattering channels is lifted. In particular, for momenta along $\mathbf{q} = \eta(\pi, \pi)$, one now has three different critical frequencies, $\Omega_c^{(i)}(\mathbf{q})$ ($i = 1, 2, 3$) [5]. $\Omega_c^{(1)}$ is the critical frequency associated with direct scattering, $\Omega_c^{(2)}$ with umklapp scattering involving $\mathbf{q} - (2\pi, 0)$ and $\mathbf{q} - (0, 2\pi)$, and $\Omega_c^{(3)}$ with umklapp scattering by $\mathbf{q} - (2\pi, 2\pi)$. The scattering momenta for \mathbf{q} close to \mathbf{Q}_0 are shown in Fig. 3(a), and $\Omega_c^{(i)}(\mathbf{q})$ for $\mathbf{q} = \eta(\pi, \pi)$ are presented in Fig. 3(b). For all of these scattering processes, $\Delta_{\mathbf{k}}$ and $\Delta_{\mathbf{k}'}$ still have opposite signs [13]. As a result, $\text{Im}\Delta\chi_0$ exhibits three discontinuous jumps at $\Omega_c^{(i)}(\mathbf{q})$, and $\text{Re}\Delta\chi_0$ diverges logarithmically at $\Omega_c^{(i)}(\mathbf{q})$ [5]. However, $\text{Im}\Delta\chi_0$ is zero only below the smallest $\Omega_c^{(i)}(\mathbf{q})$, and hence a true resonance is only possible below the smallest critical frequency. The splitting of the critical frequencies for $\mathbf{q} \neq \mathbf{Q}$ was also discussed in Ref. [14].

It follows from Fig. 3(b) that for $0.8 < \eta < 1.2$, the smallest critical frequency, $\Omega_c^{(1)}$, corresponds to direct (i.e., non-umklapp) scattering. $\Omega_c^{(1)}$ decreases away from $\eta = 1$ and eventually vanishes at $\eta = 0.8$, when direct scattering occurs between nodal points at the Fermi surface [5]. Since the exciton is necessarily located below $\Omega_c^{(1)}$, its frequency also decreases and eventually vanishes at $\eta = 0.8$. Moreover, upon approaching $\eta = 0.8$ the jump in $\text{Im}\Delta\chi_0(\mathbf{q}, \Omega_c^{(1)})$ decreases as \mathbf{k} and \mathbf{k}' approach the nodal points. Accordingly, the resonance frequency Ω_{res} moves closer to $\Omega_c^{(1)}$, and the intensity of the resonance decreases [5].

At $\mathbf{Q}_0 = 0.8(\pi, \pi)$, $\text{Im}\chi_0(\mathbf{Q}_0, \Omega)$ is non-zero for $\Omega > 0$, and one finds $\text{Im}\chi(\mathbf{Q}_0, \Omega) = \gamma_{\mathbf{Q}_0}^{SC}\Omega$ at small frequencies, where $\gamma_{\mathbf{Q}_0}^{SC} = \gamma_Q^{NS} \frac{1}{8} \frac{\pi v_F}{4v_\Delta}$ and v_Δ is the gap velocity at the nodal points. The factor $1/8$ arises since only a single (direct) scattering channel contributes to $\gamma_{\mathbf{Q}_0}^{SC}$, while eight channels contribute to γ_Q^{NS} . However, since the Fermi velocities at the nodal points are antiparallel, $\gamma_{\mathbf{Q}_0}^{SC}$ depends on v_F only through the ratio $v_F/v_\Delta \sim 20$ which compensates the small prefactor [15]. As a result, $\gamma_{\mathbf{Q}_0}^{SC}$ is comparable to γ_Q^{NS} , thus giving rise to a weak and featureless frequency dependence of $\text{Im}\chi(\mathbf{Q}_0, \Omega)$ similar to that of $\text{Im}\chi_0(\mathbf{Q}, \Omega)$ in the normal state. The vanishing of the gap in the p-h continuum at \mathbf{Q}_0 together with the large value of $\gamma_{\mathbf{Q}_0}^{SC}$ explains the experimental observation of a “silent band” in Ref. [7] (the position of which is indicated by the shaded area in Fig. 2).

For momenta $\mathbf{q} < \mathbf{Q}_0$, (i.e., $\eta < 0.8$) the nodal points cannot be connected, and a *direct* gap opens for excitations into the p-h continuum. This gap is independent of the SC gap, and given by $\Omega_c^d = \mathbf{v}_F \cdot (\mathbf{Q}_0 - \mathbf{q})$ (see dashed-dotted line in Fig. 3(b)). Due to a large $|\mathbf{v}_F|$, Ω_c^d becomes equal to $\Omega_c^{(2)}$ close to \mathbf{Q}_0 at $\mathbf{q}_d = \eta_d \mathbf{Q}$ with $\eta_d = 0.773$ (i.e., $\mathbf{Q}_0 - \mathbf{q}_d = 0.027\mathbf{Q}$ for the dispersion of Eq. (2)). For $\eta_d < \eta < 0.8$, one finds that $\text{Im}\chi_0$ vanishes below Ω_c^d , and $\text{Im}\chi_0 \sim \sqrt{\Omega - \Omega_c^d}$ for $\Omega > \Omega_c^d$. Hence, $\text{Re}\chi_0$ does not diverge at Ω_c^d , and no resonance peak exists in this region, extending the silent band. However, $\text{Re}\chi_0$ possesses a logarithmic divergence at $\Omega_c^{(2)}$, and hence it satisfies the resonance condition $\text{Re}\Delta\chi_0(\mathbf{q}, \bar{\Omega}_{res}) = \xi_{\mathbf{q}}^{-2}/g_{\mathbf{q}}$ at some frequency $\bar{\Omega}_{res}$ below $\Omega_c^{(2)}$. Once Ω_c^d crosses $\bar{\Omega}_{res}$, the damping at Ω_{res} vanishes and a true pole in $\text{Im}\chi$ occurs, leading to the appearance of the Q^* mode (open circles in Fig. 3(b)). As one moves further away from \mathbf{Q}_0 , one finds that the Q^* resonance is rapidly suppressed. This suppression arises from the rapid decrease of $\Omega_c^{(2)}$ as well as the decrease of the bare static spin susceptibility, $\chi_0(\mathbf{q}, 0)$. This behavior of $\chi_0(\mathbf{q}, 0)$ is similar to that in a system of free fermions with a circular Fermi surface, if we identify \mathbf{Q}_0 with $2\mathbf{p}_F$. Both effects lead to a rapid shift of the Q^* mode towards the edge of the p-h continuum, and to a decrease in its intensity. As a result, this resonance is only visible near \mathbf{Q}_0 .

The Q and Q^* modes are not only separated in frequency, as discussed above, but their intensity maxima are also located in different parts of the MBZ; this represents a major qualitative distinction between the two modes. In Fig. 4 we present intensity plots of $\text{Im}\chi$ as a function of momentum for $\Omega > \Omega_{res}(\mathbf{Q})$, probing the Q^* mode [Fig. 4(b)], and for $\Omega < \Omega_{res}(\mathbf{Q})$, probing the Q mode [Fig. 4(a)]. The difference is striking. While the intensity of the Q mode is largest along $\mathbf{q} = (\pi, \eta\pi)$ and $\mathbf{q} = (\eta\pi, \pi)$, the Q^* mode has its largest intensity along the diagonal direction, i.e., along $\mathbf{q} = \eta(\pi, \pi)$ and $\mathbf{q} = [(2 - \eta)\pi, \eta\pi]$. This rotation of the intensity pattern

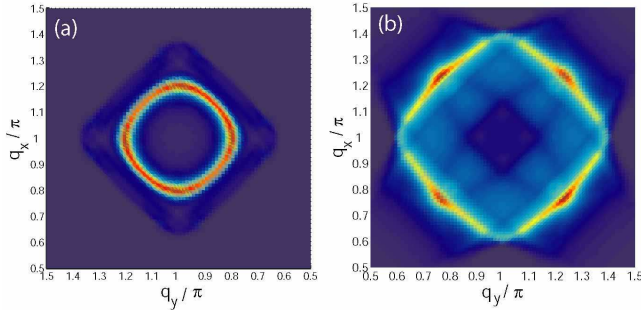


FIG. 4: (color) Intensity plot of $\text{Im}\chi$, Eq. (1), as a function of momentum (blue (red) implies a small (large) value of $\text{Im}\chi$) at: (a) 33 meV (Q mode), and (b) 57 meV (Q^* mode). The Q mode forms a distorted ring in momentum space, with intensity maxima along (π, q) . In contrast, the intensity of the Q^* mode is largest along the zone diagonal. In (b), the periodic structure of $\text{Im}\chi$ around \mathbf{Q} reflects the momentum dependence of the p-h continuum at this energy.

by 45° reflects the qualitative difference in the origin of the two modes. The intensity of the Q mode is at a maximum along $\mathbf{q} = (\pi, \eta\pi)$ and $\mathbf{q} = (\eta\pi, \pi)$, since in this case the fermions that are scattered by \mathbf{q} are located farther from the nodes than for diagonal scattering. In contrast, the Q^* mode arises from the rapid opening of a gap in the p-h continuum below \mathbf{Q}_0 , which is most pronounced along the diagonal directions of the zone. The rotation of the intensity pattern by 45° , which is the most significant distinction between the Q and Q^* modes, was observed in recent INS experiments [8, 16].

In summary, we showed that a new resonant magnetic excitation at incommensurate momenta, observed recently by inelastic neutron scattering experiments on $\text{YBa}_2\text{Cu}_3\text{O}_{6.85}$ [7] and $\text{YBa}_2\text{Cu}_3\text{O}_{6.6}$ [8], is a spin excitation arising from umklapp scattering. Its location in the zone and its frequency are determined by the momentum dependence of the p-h continuum. It is confined to a small region in \mathbf{q} just below \mathbf{Q}_0 , and is separated from the Q resonance by a “silent band” where $\text{Im}\chi$ is strongly suppressed. We also found that the intensity maxima of the two modes are rotated by 45° relative to each other.

We thank Ph. Bourges, B. Keimer, and H. Mook for discussions concerning their data. I.E. is thankful to INTAS (No. 01-0654) and RSP Superconductivity Grant No. 98014-3 for the support. D.K.M. acknowledges support from the Alexander von Humboldt foundation. A.C. acknowledges support from NSF DMR 0240238 and SFB 290. M.R.N. is supported by the US Dept. of Energy, Office of Science, under Contract No. W-31-109-ENG-38. D.K.M. and A.C. are grateful for the hospitality of the Freie Universität Berlin. D.K.M., A.C., and M.R.N. also acknowledge support from the Aspen Center for Physics where this work was completed.

*on leave from the Physics Dept., Kazan State University, 420008, Kazan, Russia.

-
- [1] J. Rossat-Mignod *et al.*, *Physica C* **185-189**, 86 (1991); H.F. Fong *et al.*, *Phys. Rev. B* **61**, 14773 (2000); P. Dai, H. A. Mook, R. D. Hunt, F. Dogan, *Phys. Rev. B* **63**, 054525 (2001).
 - [2] H.F. Fong *et al.*, *Nature (London)* **398**, 588 (1999).
 - [3] H. He *et al.*, *Science* **295**, 1045 (2002).
 - [4] H.-Y. Kee, S.A. Kivelson, and G. Aeppli, *Phys. Rev. Lett.* **88**, 257002 (2002); Ar. Abanov *et al.*, *Phys. Rev. Lett.* **89**, 177002 (2002).
 - [5] H.F. Fong *et al.* *Phys. Rev. Lett.* **75**, 316 (1995); Ar. Abanov and A.V. Chubukov, *Phys. Rev. Lett.* **83**, 1652 (1999); J. Brinckmann and P. A. Lee, *Phys. Rev. Lett.* **82**, 2915 (1999); Y.-J. Kao *et al.* *Phys. Rev. B* **61**, R11898 (2000); F. Onufrieva and P. Pfeuty, *Phys. Rev. B* **65**, 054515 (2002); D. Manske, I. Eremin, and K. H. Bennemann, *Phys. Rev. B* **63**, 054517 (2001); M.R. Norman, *Phys. Rev. B* **61**, 14751 (2000); *ibid* **63**, 092509 (2001); A. Chubukov, B. Janko and O. Tchernyshov, *Phys. Rev. B* **63**, 180507(R) (2001).
 - [6] L. Yin, S. Chakravarty, and P.W. Anderson, *Phys. Rev. Lett.* **78**, 3559 (1997); E. Demler and S.C. Zhang, *Phys. Rev. Lett.* **75**, 4126 (1995); D.K. Morr and D. Pines, *Phys. Rev. Lett.* **81**, 1086 (1998); M. Vojta and T. Ulbricht, *cond-mat/0402377* (unpublished); G.S. Uhrig *et al.*, *cond-mat/0402659* (unpublished).
 - [7] S. Pailhes *et al.*, *cond-mat/0403609* (unpublished).
 - [8] S.M. Hayden *et al.*, *Nature (London)* **429**, 531 (2004).
 - [9] For the numerical calculation of χ_0 , we employed $\delta = 2$ meV in the analytic continuation of the Greens functions $i\omega_n \rightarrow \omega + i\delta$.
 - [10] A. Damascelli, Z. Hussain, and Z.-X. Shen, *Rev. Mod. Phys.* **75**, 473 (2003).
 - [11] This expression is valid even for interacting fermions as long as the fermionic self-energy does not depend on the momentum transverse to the Fermi surface. We also assume for simplicity that Δ is independent of frequency.
 - [12] $\text{Re}\Delta\chi_0 \neq 0$ only if one includes the curvature of the dispersion in the normal state.
 - [13] For small enough q , this sign change no longer occurs. In particular, for $\Omega_c^{(2)}$, there is no sign change when q is less than the “kink” in Fig. 3(b).
 - [14] D.K. Morr and D. Pines, *Phys. Rev. B* **62**, 15177 (2000); *ibid.* *Phys. Rev. B* **61**, R6483 (2000).
 - [15] In the normal state, $\text{Im}\chi_0(\mathbf{Q}_0, \Omega)$ is finite due to the curvature of the fermionic dispersion with $\text{Im}\chi_0(\mathbf{Q}_0, \Omega) = \gamma_{\mathbf{Q}}^{NS}(v_F k_0 |\Omega|/32)^{1/2}$, where k_0 is defined via $\epsilon_{\mathbf{k}} = v_F(k_\perp + k_\parallel^2/2k_0)$. For a circular Fermi surface, $k_0 = k_F$.
 - [16] The underdoped INS data reveal a pattern in momentum space which is more spot like than the optimal doped data, both for the Q and Q^* modes. This effect can be reproduced in the RPA calculations if the Fermi surface is flattened near the node.